

Article

Characteristics of High Surface Area Molybdenum Nitride and Its Activity for the Catalytic Decomposition of Ammonia

Seo-Hyeon Baek ^{1,†}, Kyunghye Yun ^{1,†}, Dong-Chang Kang ², Hyejin An ³, Min Bum Park ³, Chae-Ho Shin ^{1,*}  and Hyung-Ki Min ^{4,*}

¹ Department of Chemical Engineering, Chungbuk National University, Chungbuk 28644, Korea; ekpeach29@gmail.com (S.-H.B.); ykh9297@gmail.com (K.Y.)

² Department of Chemical Engineering, Pohang University of Science and Technology, Pohang 37673, Korea; 88dckang@gmail.com

³ Department of Energy and Chemical Engineering, Incheon National University, Incheon 22012, Korea; hjan_95@inu.ac.kr (H.A.); mbpark@inu.ac.kr (M.B.P.)

⁴ Lotte Chemical Research Institute, Daejeon 34110, Korea

* Correspondence: chshin@chungbuk.ac.kr (C.-H.S.); pulcherrima7@gmail.com (H.-K.M.); Tel.: +82-43-261-2376 (C.-H.S.)

† These authors contributed equally to this work.

Abstract: High surface area ($>170 \text{ m}^2 \text{ g}^{-1}$) molybdenum nitride was prepared by the temperature-programmed nitridation of $\alpha\text{-MoO}_3$ with pure ammonia. The process was optimized by adjusting the experimental variables: the reaction temperature, heating rate, and molar flow rate of ammonia. The physicochemical properties of the as-formed molybdenum nitride were characterized by X-ray diffraction, N_2 sorption, transmission electron microscopy, temperature-programmed oxidation/reduction, and X-ray photoelectron spectroscopy. Of the experimental variables, the nitridation temperature was found to be the most critical parameter determining the surface area of the molybdenum nitride. When the prepared molybdenum nitride was exposed to air, the specific surface area rapidly decreased because of the partial oxidation of molybdenum nitride to molybdenum oxynitride. However, the surface area recovered to 90% the initial value after H_2 treatment. The catalyst with the highest degree of nitridation showed the best catalytic activity, superior to that of unmodified $\alpha\text{-MoO}_3$, for the decomposition of ammonia because of its high surface area.

Keywords: molybdenum nitride; ammonia decomposition; hydrogen production; nitridation; topotactic transition



Citation: Baek, S.-H.; Yun, K.; Kang, D.-C.; An, H.; Park, M.B.; Shin, C.-H.; Min, H.-K. Characteristics of High Surface Area Molybdenum Nitride and Its Activity for the Catalytic Decomposition of Ammonia. *Catalysts* **2021**, *11*, 192. <https://doi.org/10.3390/catal11020192>

Received: 24 December 2020

Accepted: 29 January 2021

Published: 2 February 2021

Publisher's Note: MDPI stays neutral with regard to jurisdictional claims in published maps and institutional affiliations.



Copyright: © 2021 by the authors. Licensee MDPI, Basel, Switzerland. This article is an open access article distributed under the terms and conditions of the Creative Commons Attribution (CC BY) license (<https://creativecommons.org/licenses/by/4.0/>).

1. Introduction

Transition metal oxides, carbides, nitrides, and phosphides are widely used as catalysts or catalyst supports [1]. Well-known oxide materials include single component oxides, such as SiO_2 , Al_2O_3 , TiO_2 , V_2O_5 , MoO_3 , and WO_3 , and their combinations have been used as catalysts and catalyst supports for reactions such as metathesis, isomerization, hydrogenation, and partial oxidation [2]. In addition, transition metal nitrides, such as Si_3N_4 , AlN , TiN , VN , Mo_2N , and $\text{WN}/\text{W}_2\text{N}$, and carbides, such as SiC , Al_4C_3 , TiC , VC , Mo_2C , and $\text{WC}/\text{W}_2\text{C}$, have been used in cutting tools and refractory materials owing to their high thermal and chemical stabilities, as well as mechanical strengths [3]. Thus, because of their remarkable thermal and chemical stabilities, these materials are potential supports or catalysts for use in heterogeneous catalysis. However, the application of transition metal nitrides and carbides has been limited because of their low specific surface areas, which are a result of sintering during their high-temperature synthesis [4,5]. To use these transition metal nitrides and carbides as catalysts or catalyst supports, it is necessary to maintain a high surface area to increase the reactant–catalyst contact as much as possible. Volpe and Boudart reported the preparation of high surface area Mo_2N and W_2N

through the topotactic nitridation of MoO_3 and WO_3 with NH_3 at high temperatures [6]. Subsequently, the prepared transition metal nitride compounds were reacted under a CH_4/H_2 atmosphere to prepare carbide counterparts with a high surface area [7]. Since then, various attempts have been made to synthesize high surface area nitride/carbide materials [8–10]. For example, binary molybdenum nitrides, such as $\text{Fe}_3\text{Mo}_3\text{N}$, $\text{Co}_3\text{Mo}_3\text{N}$, and $\text{Ni}_3\text{Mo}_3\text{N}$, have been prepared by adding Fe, Co, and Ni, respectively, to high surface area Mo_2N to improve its catalytic activity and stability [11–14].

As a hydrogen storage medium and carrier, ammonia has a relatively low specific energy cost, especially compared to its alternatives [15–17]. Thus, the catalytic decomposition of ammonia with energy efficient manner is a key technology to utilize it as a hydrogen carrier. Ru-based catalysts are most active for the decomposition of ammonia and are capable of completely converting ammonia to nitrogen at 450 °C [18,19], but Ru is expensive. Thus, various attempts have been made to replace these precious metal catalysts [20–23]. As alternative catalyst materials, transition metal nitrides have been widely applied in chemical reactions, such as ammonia synthesis [24–26], carbazole hydrodenitrogenation [27], indole hydrodenitrogenation [28], hydrazine decomposition [29], and direct NO decomposition [30]. Stoichiometric Mo_2N exists as crystalline γ -, δ -, and β -phases depending on the synthesis conditions, and, in general, molybdenum nitride synthesized from α - MoO_3 is γ - Mo_2N [31,32].

In this study, molybdenum nitride having a high surface area was prepared by the topotactic conversion of α - MoO_3 by ammonia treatment at high temperature, and the catalytic activity of these materials for the decomposition of ammonia were investigated. The reaction parameters, such as the molar hourly space velocity (MHSV, which is defined as the molar rate of pure ammonia per mole of α - MoO_3), reaction temperature, or ramping rate most influencing the surface area of the molybdenum nitride prepared was systematically investigated and correlated with the performance of catalytic ammonia decomposition. The prepared molybdenum nitride was characterized by various techniques, and its stability under an oxidizing, reducing, and inert atmosphere was examined.

2. Results and Discussion

Figure 1a shows the plots of NH_3 decomposition and H_2 and H_2O production during temperature-programmed nitridation, as well as the reduction of α - MoO_3 and MoO_2 , as a function of reaction temperature. H_2O , which is generated by the reduction of oxides by NH_3 , was detected from ca. 320 °C, and the evolution of H_2 via the decomposition of NH_3 was observed at ca. 400 °C. The evolution of H_2 over both oxides started from the peak temperature in the H_2O evolution curves, indicating that the decomposition of NH_3 proceeds over nitrated α - MoO_3 (γ - Mo_2N). Dewangan et al. reported that the formation of γ - Mo_2N by the nitridation of α - MoO_3 with NH_3 proceeds via an intermediate γ - $\text{Mo}_2\text{O}_x\text{N}_{1-x}$ or MoO_2 phase [32]. Thus, the hydrogen produced by the initial dissociation of NH_3 was not detected and was mostly consumed during the reduction of both oxides. In addition, the decomposition of NH_3 and generation of H_2 over α - MoO_3 require higher temperatures than MoO_2 because of the formation of an intermediate γ - $\text{Mo}_2\text{O}_x\text{N}_{1-x}$ phase from α - MoO_3 .

The reaction parameters affecting the Brunauer–Emmett–Teller (BET) surface area, total pore volume, and average pore diameter during the nitridation of α - MoO_3 were investigated by changing the nitridation temperature, heating rate, and MHSV (Figure 1b–d, respectively). As shown in Figure 1b, the BET surface area of α - MoO_3 increased proportionally with increase in nitridation temperature, reaching its maximum value of $150 \text{ m}^2 \text{ g}^{-1}$ at 630 °C; this is approximately 50 times higher than that ($3 \text{ m}^2 \text{ g}^{-1}$) of pristine α - MoO_3 . In line with the increase in the BET surface area, the total pore volume of α - MoO_3 increased proportionally to the nitridation temperature up to 770 °C, subsequently decreasing rapidly because of the phase transformation of γ - Mo_2N to the other phase, such as β - Mo_2N . Wei et al. reported the transformation of γ - Mo_2N to β - Mo_2N at 600 °C and β - Mo_2N to metallic Mo at around 880 °C based on the observation of N_2 release in their temperature-

programmed reduction (TPR) experiments under flowing H_2 [33]. Thus, the reduction of the specific surface area at nitridation temperatures higher than $630\text{ }^\circ\text{C}$ can be attributed to the formation of the $\beta\text{-Mo}_2\text{N}$ phase. However, a continuous increase in the total pore volume up to $770\text{ }^\circ\text{C}$ was observed, probably because of the formation of mesopores during the partial transformation of $\gamma\text{-Mo}_2\text{N}$ to $\beta\text{-Mo}_2\text{N}$ [34]. The differentiation of $\gamma\text{-Mo}_2\text{N}$ and $\beta\text{-Mo}_2\text{N}$ by X-ray diffraction is quite difficult because of the heavy overlap of the characteristic peaks; however, the BET surface areas of $\gamma\text{-Mo}_2\text{N}$ and $\beta\text{-Mo}_2\text{N}$ fall into the range of $40\text{--}145$ and $2\text{--}17\text{ m}^2\text{ g}^{-1}$, respectively [25,35,36]. Thus, it can be reasonably speculated that the phase change of $\gamma\text{-Mo}_2\text{N}$ to $\beta\text{-Mo}_2\text{N}$ occurred at the temperatures higher than $630\text{ }^\circ\text{C}$. The rapid increase in the average pore diameter with associated reduction in the surface area and pore volume over the samples nitrided at temperatures higher than $800\text{ }^\circ\text{C}$ is a result of the formation of metallic Mo particles. This can be further supported by the observation of X-ray diffraction peaks corresponding to metallic Mo at the temperatures higher than $800\text{ }^\circ\text{C}$, as shown in Table S1. In fact, the heating rate during high-temperature treatment of oxide materials is an important factor determining the surface area and particle size [2]. Figure 1c shows the textural properties (i.e., BET surface area, total pore volume, and average pore diameter) of $\alpha\text{-MoO}_3$ nitrided in flowing NH_3 at $630\text{ }^\circ\text{C}$ and a MHSV of 6.2 h^{-1} at different heating rates ($30\text{--}240\text{ }^\circ\text{C h}^{-1}$). For the nitridation of $\alpha\text{-MoO}_3$ in flowing NH_3 , a low heating rate at temperatures below $450\text{ }^\circ\text{C}$ is advantageous for the generation of $\gamma\text{-Mo}_2\text{O}_x\text{N}_{1-x}$ and $H_x\text{MoO}_3$ rather than MoO_2 [32]. Under these conditions, the H_2 formed by the dissociation of NH_3 diffuses into the $\alpha\text{-MoO}_3$ lattice and produces the $H_x\text{MoO}_3$ phase by a topotactic reaction in which the loosely held double-thick layers of $[MoO_6]$ octahedra in $\alpha\text{-MoO}_3$ are broken by H_2 insertion [37]. On the other hand, the fast heating of $\alpha\text{-MoO}_3$ below $450\text{ }^\circ\text{C}$ disturbs the diffusion of H_2 into the $\alpha\text{-MoO}_3$ lattice, and, as a result, the decomposition of $\alpha\text{-MoO}_3$ to MoO_2 dominates. As shown in Figure 1c, the surface area of nitrided $\alpha\text{-MoO}_3$ was maintained higher than $150\text{ m}^2\text{ g}^{-1}$ when a heating rate of less than $120\text{ }^\circ\text{C h}^{-1}$ was used but steadily reduced at higher heating rates. This implies that the diffusion of H_2 is limited at heating rates higher than $120\text{ }^\circ\text{C h}^{-1}$, resulting in the decomposition of $\alpha\text{-MoO}_3$ to MoO_2 . This result is also well correlated with the rapid increase in the average pore diameter of this material at heating rates higher than $120\text{ }^\circ\text{C h}^{-1}$. Unlike the changes in surface area and average pore diameter, the total pore volume of nitrided $\alpha\text{-MoO}_3$ hardly changed over the entire range of heating rates. Figure 1d shows the changes in the BET surface area, total pore volume, and average pore diameter of $\alpha\text{-MoO}_3$ nitrided with NH_3 at $630\text{ }^\circ\text{C}$ as a function of MHSV. The $\alpha\text{-MoO}_3$ nitrided with NH_3 at a low MHSV of 10 h^{-1} has a relatively low surface area and total pore volume, probably because of the thermal reduction of $\alpha\text{-MoO}_3$ to MoO_2 at this reaction temperature. Spevack and McIntyre also observed the thermal reduction of $\alpha\text{-MoO}_3$ to MoO_2 at $600\text{ }^\circ\text{C}$ using Raman spectroscopy [38]. The surface area of nitrided $\alpha\text{-MoO}_3$ gradually increased with increasing MHSV and leveled off at MHSV values higher than 40 h^{-1} . In addition, the total pore volume of the nitrided sample rapidly increased until the MHSV reached 20 h^{-1} and was slightly reduced at higher MHSV.

The theoretical mass reduction in the transformation of $\alpha\text{-MoO}_3$ to $\gamma\text{-Mo}_2\text{N}$ is 28.5 wt.%, and the nitrogen content in $\gamma\text{-Mo}_2\text{N}$ is 6.8 wt.%. As shown in Table S1, the mass reduction occurred below the theoretical value for all nitride samples obtained after nitridation, and, in most cases, the MoO_2 phase was detected. Thus, to prevent the rapid surface oxidation of the nitrided sample on exposure to air, the sample was passivated with 1% O_2/Ar at room temperature, and the weight difference between the theoretical and practical values of the sample can be explained by oxygen adsorption and diffusion into the nitride samples. Above a nitridation temperature of $700\text{ }^\circ\text{C}$, the MoO_2 phase was no longer detected, and only the $\gamma\text{-Mo}_2\text{N}$ phase was observed by X-ray diffraction (XRD) analysis (Figure S1 and Table S1). The lattice parameter of the sample nitrided at $700\text{ }^\circ\text{C}$ was similar (0.4166 nm) to that of stoichiometric $\gamma\text{-Mo}_2\text{N}$ ($a = 0.4165\text{ nm}$), which has a face-centered cubic (fcc) structure [31,32]. Above a nitridation temperature of $800\text{ }^\circ\text{C}$, metallic Mo was detected by XRD analysis, and this was likely formed by the partial decomposition of $\gamma\text{-Mo}_2\text{N}$

(Table S1). This formation of metallic Mo caused a rapid decrease in the surface area and total pore volume, and the porous nature of the sample was lost.

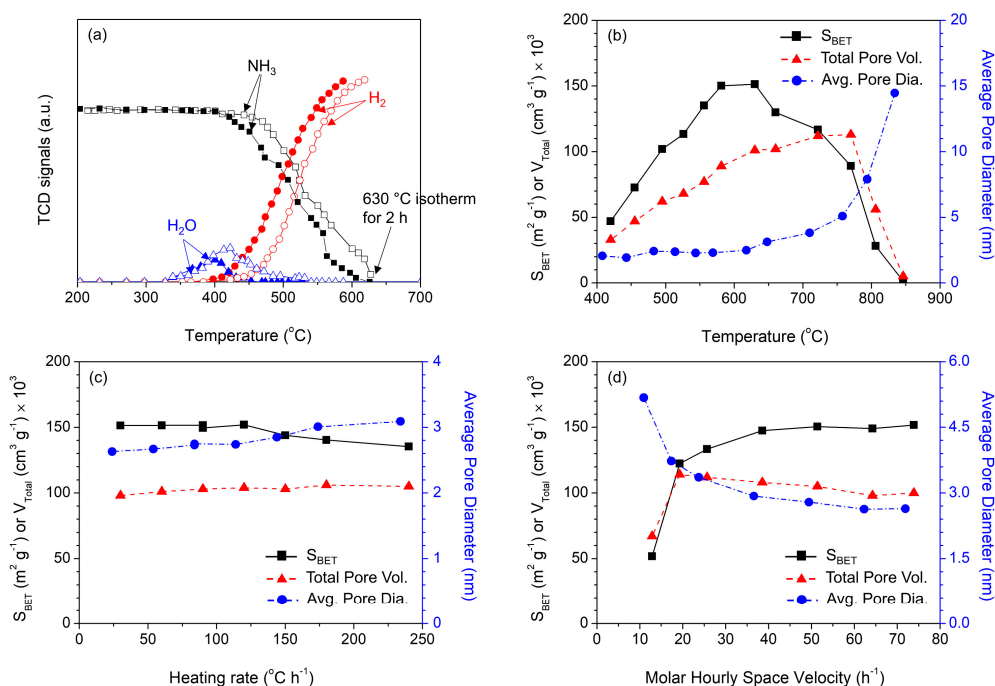


Figure 1. (a) NH₃ decomposition and production of H₂O and H₂ during the temperature-programmed nitridation of α -MoO₃ (open symbols) and MoO₂ (closed symbols) from 200 to 630 °C for 2 h. Standard nitridation conditions were an MHSV of 64.2 h⁻¹ (10 L h⁻¹ for 1 g α -MoO₃) at heating rates of 200 °C h⁻¹ to 200 °C and then 30 °C h⁻¹ to 630 °C followed by maintenance at this temperature for 2 h. (b–d) Changes in textural properties of nitride samples obtained after the nitridation of α -MoO₃ as a function of (b) reaction temperature at a heating rate of 30 °C h⁻¹ and MHSV of 64.2 h⁻¹, (c) heating rate (heating to 630 °C at an MHSV of 64.2 h⁻¹), and (d) MHSV (heating at a rate of 90 °C h⁻¹).

Figure 2 shows the N₂ adsorption–desorption isotherms of α -MoO₃ and the analogous samples nitrided at different temperatures for 7 h. The α -MoO₃ sample shows a typical type II isotherm, which is characteristic of non-porous materials [39]. This is further supported by its very low BET surface area (2.8 m² g⁻¹) and total pore volume (0.007 cm³ g⁻¹). However, the shape of the N₂ adsorption–desorption isotherm of nitrided α -MoO₃ gradually changed to type IV, characteristic of a mesoporous material, as the nitridation temperature increased from 450 to 700 °C, and the hysteresis loop related to the narrow slit-type pores was observed over all nitrided α -MoO₃. The maximum BET surface area (145 m² g⁻¹) and total pore volume (0.106 cm³ g⁻¹) were observed for α -MoO₃ nitrided at 650 °C. The maximum Barrett–Joyner–Halenda (BJH) pore diameter calculated from the N₂ adsorption branch also gradually increased from 1.2 to 2.2 nm with the increase in nitridation temperature.

Figure 3 shows the results of simultaneous thermogravimetric (TG)/differential thermal analysis (DTA)–mass spectrometry (MS) analyses of the nitrided α -MoO₃ (i.e., γ -Mo₂N) under inert, oxidizing, and reducing atmospheres (He, O₂, and 20% H₂/He, respectively). The TG-DTA traces shown in Figure 3a,b contain three steps of weight loss and changes in the heat flow in flowing O₂: 0–250, 250–700, and 700–900 °C, corresponding to the exothermic oxidation of γ -Mo₂N to γ -Mo₂O_xN_{1-x} or MoO₂ (14% mass increase), total oxidation to α -MoO₃ (5% mass increase), and melting and evaporation of α -MoO₃, respectively. The sharp endothermic peak observed in the DTA curve around 800 °C represents the phase transformation of solid α -MoO₃ (melting point = 795 °C) to the liquid phase. As shown in Figure 3c, massive consumption of O₂ (m/z = 32) and evolution of N₂ (m/z = 28) at ca. 450 °C in an oxidizing atmosphere were observed by quadrupole mass spectrometry

(QMS), indicating that the total oxidation of $\gamma\text{-Mo}_2\text{O}_x\text{N}_{1-x}$ to $\alpha\text{-MoO}_3$ occurred at this temperature. This is further confirmed by the fact that only peaks corresponding to $\alpha\text{-MoO}_3$ were observed in the XRD pattern (Figure S2c) of $\gamma\text{-Mo}_2\text{N}$ treated at 700 °C in flowing 5% O_2/He ($100\text{ cm}^3\text{ min}^{-1}$). The theoretical mass increases for the oxidation of $\gamma\text{-Mo}_2\text{N}$ to MoO_2 and $\alpha\text{-MoO}_3$ are 24.3% and 39.8%, respectively. The actual mass increase of less than 20% under an O_2 atmosphere is probably due to the partial oxidation of the prepared $\gamma\text{-Mo}_2\text{N}$ to $\gamma\text{-Mo}_2\text{O}_x\text{N}_{1-x}$ or MoO_2 , especially in the surface region during the passivation process. The mass losses observed up to 400 °C under H_2 and He atmospheres mainly originate from the reaction adsorbed ammonia on the partially oxidized $\alpha\text{-MoO}_3$ ($\text{MoO}_3\cdot\text{NH}_3 \rightarrow \gamma\text{-MoO}_x\text{N}_{1-x}$), and the mass reduction at temperatures higher than 600 °C is probably due to the phase transformation of $\gamma\text{-Mo}_2\text{N}$ to $\beta\text{-Mo}_2\text{N}$, which is well correlated with the decrease in the surface area of this material, as shown in Figure 1b. However, as shown in Figure S2b, a significant amount of the MoO_2 phase was observed after treatment with $\gamma\text{-Mo}_2\text{N}$ in a flow of pure He ($100\text{ cm}^3\text{ min}^{-1}$), probably caused by the decomposition of surface $\gamma\text{-Mo}_2\text{O}_x\text{N}_{1-x}$ formed during passivation in 1% O_2/He to MoO_2 . The generation of nitrogen-containing compounds (i.e., NO , NO_2 , and N_2O) and H_2 below 300 °C in the He atmosphere supports the presence of reaction with adsorbed ammonia and lattice oxygen (Figure 3d). In addition, the increase in N_2 release at temperatures higher than 600 °C confirms the phase transformation to the nitrogen-deficient $\beta\text{-Mo}_2\text{N}$ phase, and this change was more significant under the reducing conditions (20% H_2/He), resulting in the higher weight loss shown in Figure 3a.

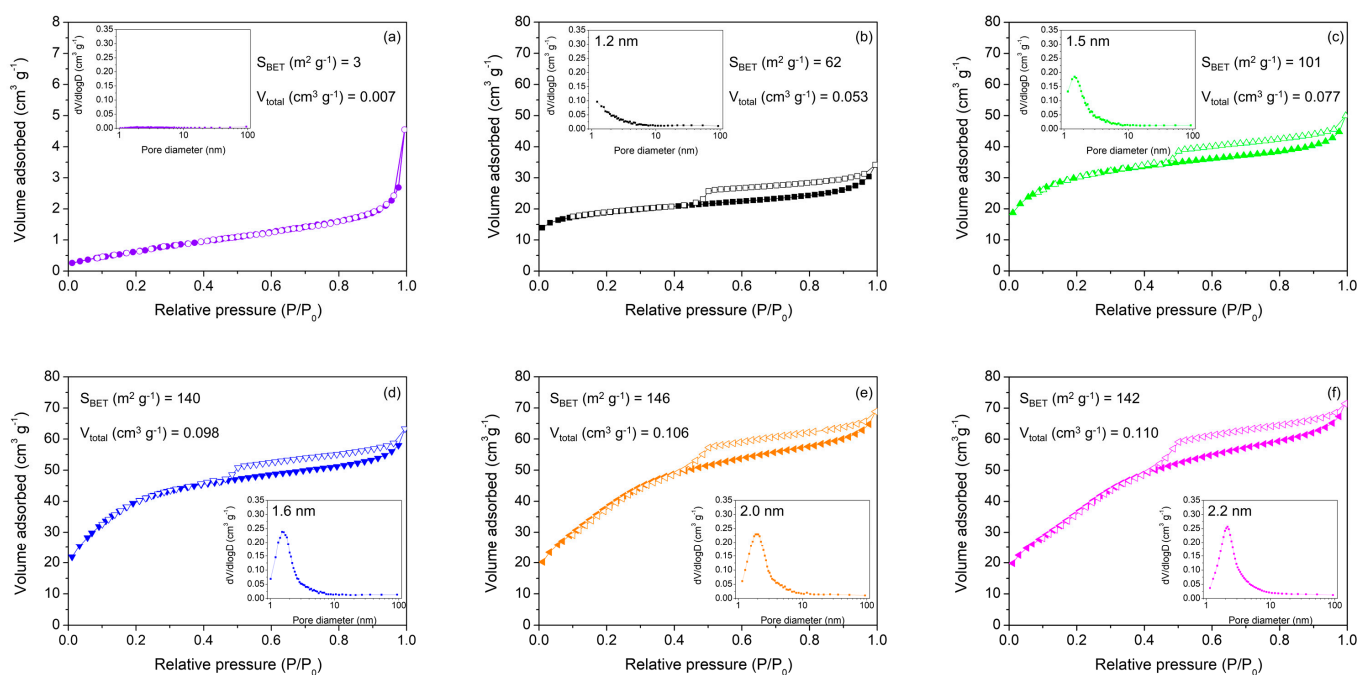


Figure 2. N_2 adsorption–desorption isotherms of (a) $\alpha\text{-MoO}_3$ and nitrided samples prepared by nitridation of $\alpha\text{-MoO}_3$ in pure ammonia flow at (b–f) 450, 550, 600, 650, and 700 °C, respectively. Nitridation conditions: pure ammonia flow rate of 3.4 L h^{-1} for 0.3 g $\alpha\text{-MoO}_3$ at a heating rate of 200 °C h^{-1} to 200 °C and, then, 60 °C h^{-1} to the final temperature, followed by maintenance at that temperature for 7 h. Insets show Barrett–Joyner–Halenda pore size distribution calculated from adsorption branch.

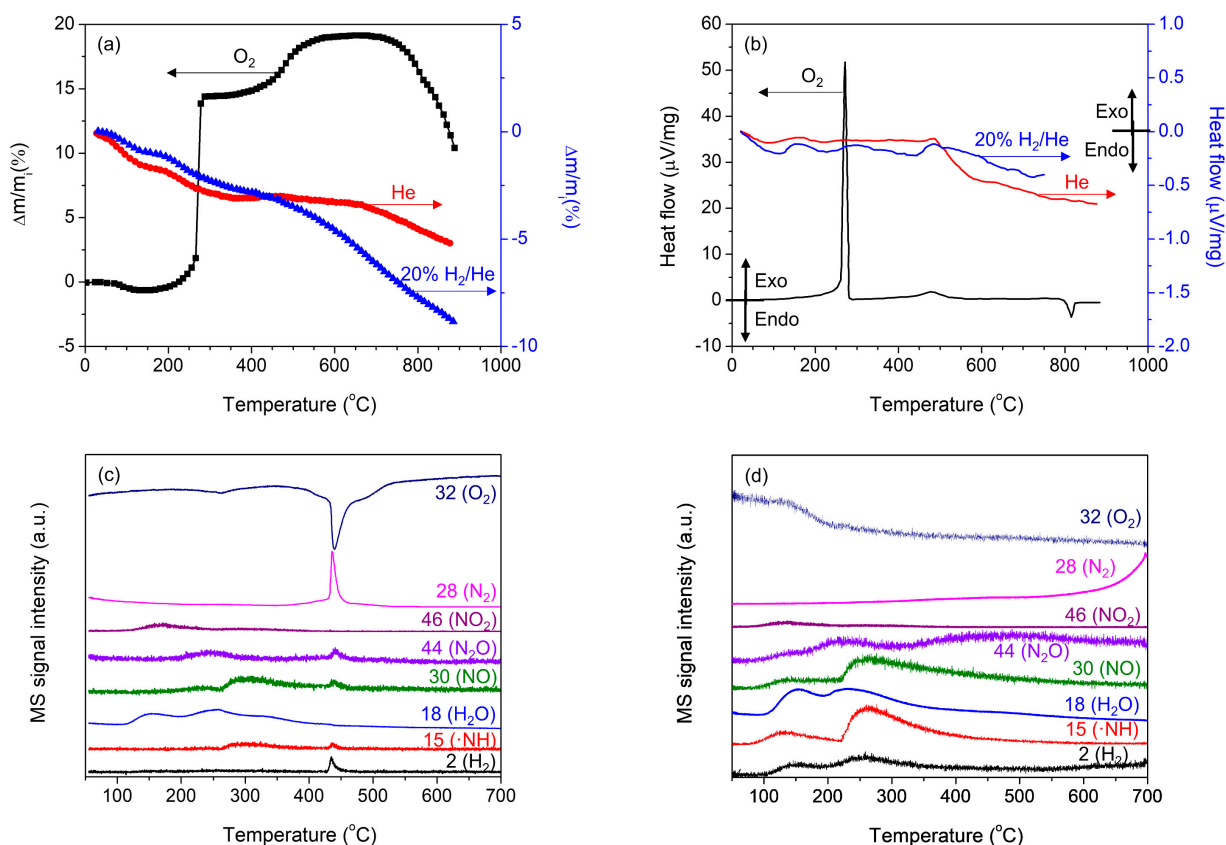


Figure 3. (a) TGA and (b) DTA curves of γ -Mo₂N in flowing helium, pure O₂, and 20% H₂/He (50 cm³ min⁻¹). Evolution of fragment ions observed by QMS during the temperature-programmed decomposition of γ -Mo₂N in flowing (c) 5% O₂/He (100 cm³ min⁻¹) and (d) pure He. This nitride sample was obtained by the nitridation of α -MoO₃ at a reaction temperature of 700 °C for 7 h at a heating rate of 60 °C h⁻¹ in flowing ammonia (10 L h⁻¹ for 1 g of α -MoO₃, i.e., MHSV = 64.2 h⁻¹).

Figure 4 shows the transmission electron microscopy (TEM) images and selected area electron diffraction (SAED) patterns of α -MoO₃ and its nitrided analogs prepared at different temperatures (550–700 °C). α -MoO₃ has plate-like morphology with an orthorhombic crystal lattice ($a = 3.96$, $b = 13.86$, and $c = 3.70$ Å) [40]. Because the nitridation proceeds at high temperatures, the generation of new pores observed in the samples is probably due to the extraction of lattice oxygen from the crystalline oxynitride phase. Volpe and Boudart [6] and Jagers [5] reported that α -MoO₃ is transformed to γ -Mo₂N under an NH₃ atmosphere via a reaction pathway in which γ -Mo₂O_xN_{1-x} or MoO₂ are reaction intermediates. The reaction pathway for α -MoO₃ nitridation is mainly dependent on the heating conditions (i.e., temperature and heating rate) [32,41]. In addition, γ -Mo₂O_xN_{1-x} is known to be transformed to γ -Mo₂N at a relatively low nitridation temperature (ca. 500 °C), whereas MoO₂ starts to react with NH₃ only at temperatures higher than 657 °C and is completely converted to γ -Mo₂N at 785 °C [6,31]. This is further supported by the observation of characteristic peaks corresponding to pure γ -Mo₂N at 700 °C, as shown in Figure S1.

As shown in Figure 4a, the SAED image of α -MoO₃ clearly shows reflections corresponding to the (100), (101), and (001) facets along the [010] direction [5]. After the transformation of α -MoO₃ to the fcc-structured γ -Mo₂O_xN_{1-x} by nitridation at high temperatures, reflections corresponding to the (002), (020), and (022) facets were also observed along the [100] direction [11,32]. Energy dispersive X-ray spectroscopy (EDS) mapping (Figure 4f) shows the uniform distribution of nitrogen on the γ -Mo₂N sample prepared at 700 °C by nitridation and also indicates the presence of molybdenum oxynitrides, which are generated during the passivation process. However, the large amount of oxygen observed

in the EDS maps of γ -Mo₂N prepared at 700 °C suggests the presence of XRD-invisible MoO₂ clusters in the sample.

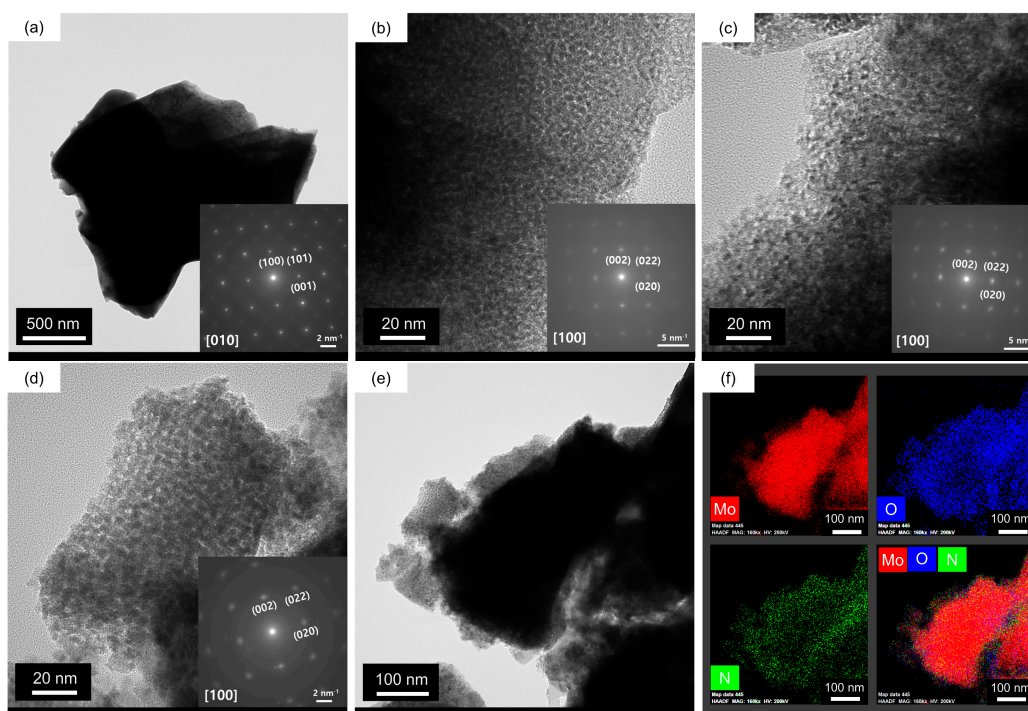


Figure 4. TEM images and SAED patterns of (a) commercial α -MoO₃ and nitrated samples treated at (b–d) 550, 600, and 700 °C, respectively; (e) α -MoO₃ and nitrated samples treated at 700 °C; and (f) EDS mapping of the nitrated sample shown in (e). Nitridation conditions: pure ammonia flow rate of 3.4 L h^{−1} for 0.3 g α -MoO₃ (MHSV = 72 h^{−1}) at heating rates of 200 °C h^{−1} to 200 °C and 60 °C h^{−1} to the final temperature, followed by maintenance at that temperature for 7 h.

To examine the stability of γ -Mo₂N under oxidizing conditions, a sample was exposed to air for up to 60 days, and the textural properties are compared in Figure 5. Compared to the initial surface area (120 m² g^{−1}) of γ -Mo₂N prepared at 700 °C for 7 h, those of the samples exposed to air gradually decreased over time, as did their total pore volumes. After 60 days, we measured the N₂ adsorption–desorption isotherm of the γ -Mo₂N sample, which revealed a change to a type II nonporous material, as well as reductions in the surface area and total pore volume of 88% and 81%, respectively, compared to the initial values. This is a result of the diffusion of oxygen into the nitride crystal lattice, which results in the formation of molybdenum oxynitride and the observed reduction in pore volume and specific surface area. After exposure to air for seven days, the initial γ -Mo₂N phase did not change significantly, as shown by the XRD analysis, which contained no peaks corresponding to molybdenum oxide phases (Figure S3). However, after air exposure for seven days, the reflection corresponding to the (111) facet shifted from 37.4° to 37.2° in 2θ . This small shift ($\Delta = 0.2^\circ$) indicates the expansion of the fcc unit cell from 0.4163 to 0.4180 nm. This volume expansion induced by oxygen diffusion into bulk γ -Mo₂N causes pore blocking and, finally, the transformation to γ -Mo₂O_xN_{1-x}, which results in a decrease in the surface area and total pore volume. However, the oxynitride sample exposed to air recovered the textural properties of the initial nitride (by more than 90% the initial values) after H₂ treatment at 500 °C for 2 h (Figure S4).

As shown in Figure 6, the distribution of Mo, N, and O in the γ -Mo₂N sample exposed to air for three days was characterized by X-ray photoelectron spectroscopy (XPS) depth profiling analysis. As the sputtering time of the Ar ion beam increased, the concentration of Mo increased and those of N and O decreased. The initial surface ratios of N/Mo and O/Mo in the samples are 0.7 and 0.4, respectively, and these ratios continuously decreased

with the increase in sputtering time. The high O/Mo ratio, especially in the surface region, indicates the oxidation of the γ -Mo₂N surface during the passivation with air. As Ar ion sputtering proceeded, the ratio of N/Mo and O/Mo gradually decreased and approached the values of Mo₂N_{0.7}O_{0.3}.

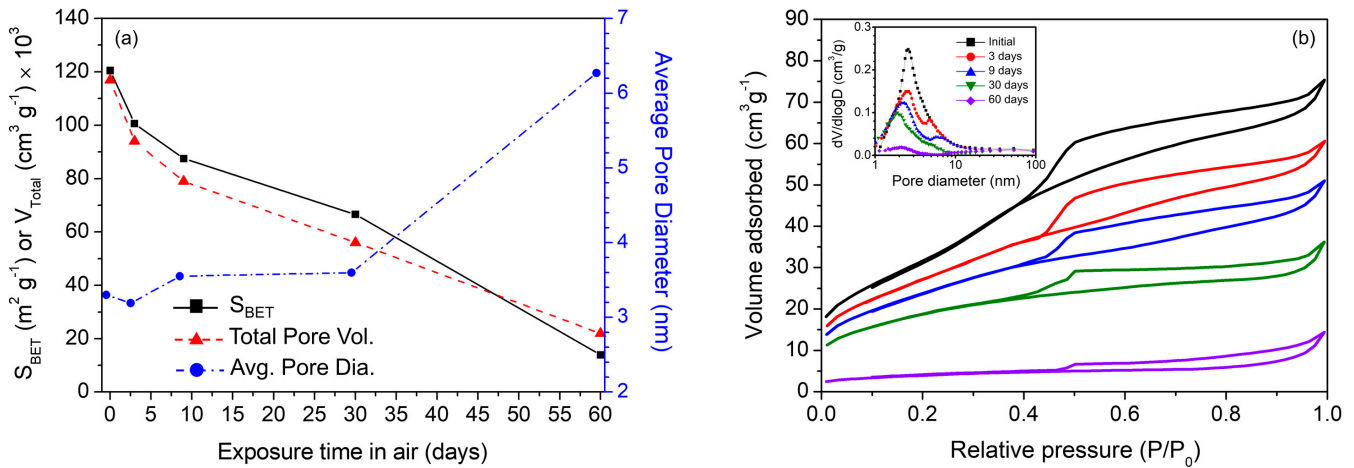


Figure 5. Changes in (a) textural properties and (b) N_2 adsorption–desorption isotherms of nitride sample as a function of exposure time in air. The inset image shows the BJH pore size distribution calculated from the adsorption branch. The nitride samples were prepared by heating 1 g α -MoO₃ at 700 °C for 7 h at heating rates of 200 °C h^{−1} to 200 °C and 60 °C h^{−1} to the final temperature in pure ammonia at a flow rate of 3.4 L h^{−1} (MHSV = 21.6 h^{−1}).

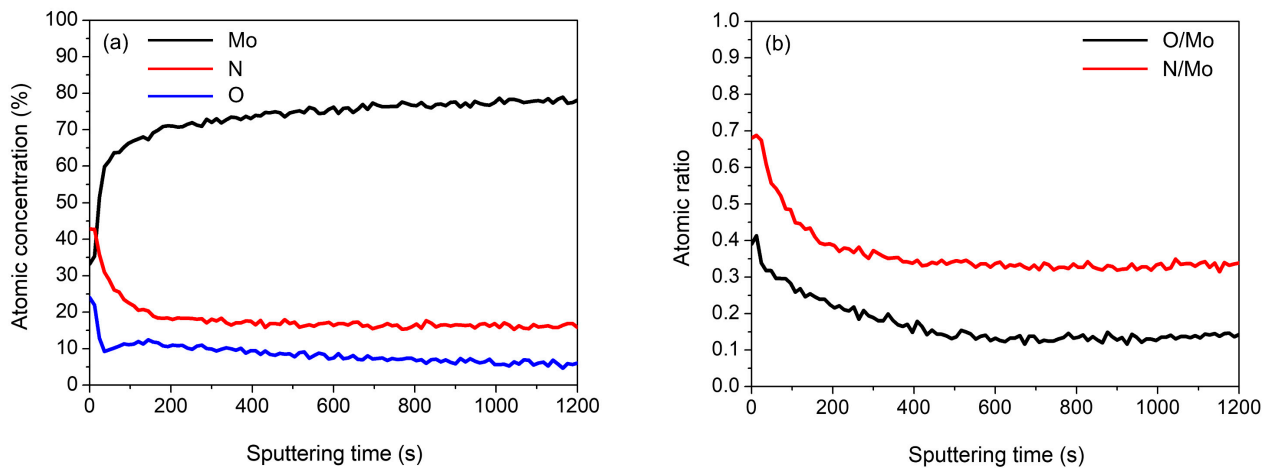


Figure 6. (a) X-ray photoelectron spectroscopy depth profiles of the major elements in γ -Mo₂N, and (b) O/Mo and N/Mo atomic ratios as a function of Ar ion sputtering time. Depth profiles were obtained by Ar ion sputtering at 0.03 nm s^{−1}. γ -Mo₂N obtained by temperature-programmed nitridation of 1.0 g α -MoO₃ at 700 °C for 7 h in pure NH₃ at a flow rate of 3.4 L h^{−1}.

The XPS results are shown in Figure 7 and Table 1. XPS measurements were performed to investigate the degree of nitridation, reduction of MoO₃, and the oxidation state of Mo with respect to the increase in nitridation temperature. The N 1s peak in the spectra was deconvoluted into three peaks: O-N, NH₃, and NH₄⁺ species centered at 397.4–397.7, 399.0–399.4, and 401.2–401.3 eV, respectively, and an overlapped Mo 3p_{3/2} peak (395.2–395.6 eV) was also observed [42,43]. The binding energy of Mo 3p_{3/2} (398.7 eV) in the unmodified α -MoO₃ shifted to lower energy after high-temperature nitridation because of the changes in the oxidation state (Mo⁶⁺ → Mo⁶⁺, Mo⁵⁺, and Mo⁴⁺) and electroneg-

activity (3.44 \rightarrow 3.04, Pauling scale) of the bonding elements. In addition, the intensities of the peaks corresponding to Mo 3p_{3/2} and O-N increased as high-temperature nitridation proceeded because of the increased proportion of Mo in Mo₂N compared to that in α -MoO₃ and the presence of γ -Mo₂O_xN_{1-x}. On the other hand, the peak intensities of adsorbed species, such as NH₃ and NH₄⁺, were reduced at higher nitridation temperatures because desorption was easier. The O 1s peaks in the spectra were deconvoluted into three peaks corresponding to O₂⁻ (530.6–530.7 eV), OH⁻ (531.8–531.9 eV), and O-N (532.9–533.1 eV) species originating from α -MoO₃, adsorbed H₂O, and γ -Mo₂O_xN_{1-x}, respectively [44]. As the nitridation temperature increased, the atomic concentration of O₂⁻ and OH⁻ decreased, whereas that of O-N increased. However, of the three components, the peak corresponding to O₂⁻ was dominant, suggesting the formation of oxide layers after passivation with dilute O₂ and the presence of XRD-invisible MoO₂ clusters. The Mo 3d peak was deconvoluted into five peaks, representing Mo⁶⁺, Mo⁵⁺, Mo⁴⁺, Mo-N, and Mo-OH centered at 232.5–232.8, 230.7–230.8, 229.7, 228.9–229.0, and 233.6–233.8 eV, respectively [45,46]. As the nitridation temperature was increased, the atomic concentration of Mo⁶⁺ decreased, whereas that of Mo-N increased. Moreover, the peak of Mo-OH was drastically reduced after nitridation at high temperatures.

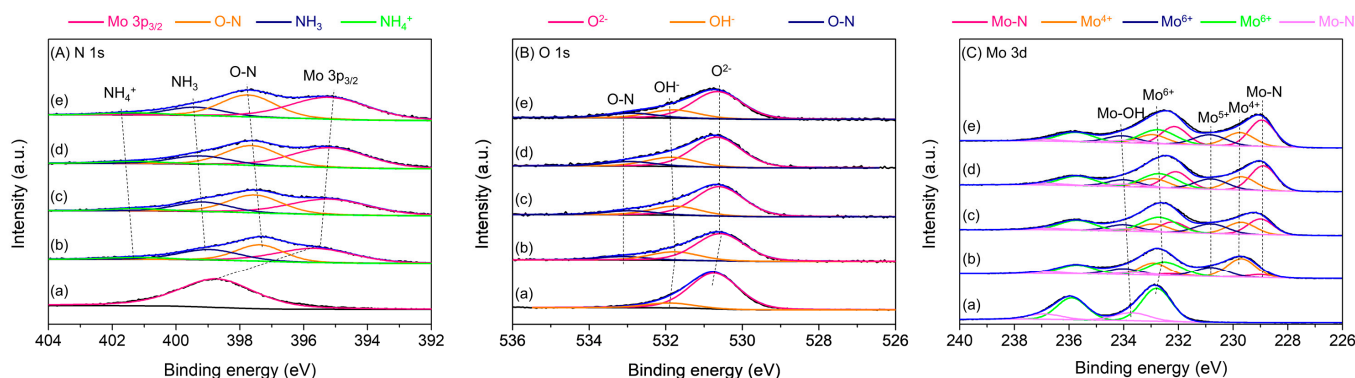


Figure 7. (A) N 1s and Mo 3p_{3/2}, (B) O 1s, and (C) Mo 3d XPS spectra of (a) α -MoO₃ and molybdenum nitride samples prepared by nitridation of α -MoO₃ at (b–e) 550, 600, 650, and 700 °C, respectively, in pure ammonia flow.

Table 1. Binding energies and atomic percentages obtained from the XPS analyses of (a) α -MoO₃ and molybdenum nitrides prepared at (b–e) 550, 600, 650, and 700 °C, respectively.

Sample	N 1s				O 1s			Mo 3d				
	Binding Energy (eV), (at.%)				Binding Energy (eV), (at.%)			Binding Energy (eV), (at.%)				
	Mo 3p _{3/2}	O-N	NH ₃	NH ₄ ⁺	O ₂ ⁻	OH ⁻	O-N	Mo-N	Mo ⁴⁺	Mo ⁵⁺	Mo ⁶⁺	Mo-OH
(a) MoO ₃	398.7 (100)	-	-	-	530.7 (88.1)	531.9 (11.9)	-	-	-	-	232.8 (77.8)	233.7 (22.2)
(b) MN (550) ¹	395.6 (41.9)	397.4 (29.5)	399.0 (24.1)	401.2 (4.5)	530.6 (69.4)	531.8 (21.7)	533.1 (8.9)	229.0 (5.1)	229.7 (36.5)	230.8 (20.5)	232.5 (32.7)	233.6 (5.2)
(c) MN (600)	395.2 (44.0)	397.5 (33.6)	399.2 (17.9)	401.2 (4.5)	530.6 (69.2)	531.8 (21.1)	532.9 (9.7)	229.0 (24.2)	229.7 (20.5)	230.8 (18.7)	232.7 (31.5)	233.8 (5.1)
(d) MN (650)	395.2 (46.9)	397.6 (33.8)	399.2 (15.1)	401.3 (4.2)	530.7 (68.8)	531.9 (20.8)	532.9 (10.4)	228.9 (32.7)	229.7 (19.7)	230.8 (17.2)	232.7 (25.5)	233.8 (4.9)
(e) MN (700)	395.2 (49.4)	397.7 (34.1)	399.4 (13.1)	401.3 (3.4)	530.7 (68.1)	531.8 (20.5)	532.9 (11.4)	228.9 (34.2)	229.7 (19.3)	230.7 (17.1)	232.7 (25.0)	233.8 (4.4)

¹ Values in parentheses denote the nitridation temperature in degrees Celsius.

The conversions of NH_3 during the nitridation of $\alpha\text{-MoO}_3$ at various temperatures were shown in Figure 8. It is obvious that the nitridation of $\alpha\text{-MoO}_3$ and catalytic decomposition of NH_3 over nitrated $\alpha\text{-MoO}_3$ proceed with the concurrent manner, and their performances are increases with the elevation of temperature. However, a sharp increase of NH_3 conversion was observed between 550 and 600 °C, probably due to the facilitated nitridation of $\alpha\text{-MoO}_3$. As shown in Figure 1b, the BET surface areas of nitrated $\alpha\text{-MoO}_3$ was almost proportional to the temperatures up to 600 °C, while no specific correlation between the surface area and the conversion of NH_3 was observed. However, the atomic content of Mo-N species in Mo 3d XPS analysis (Table 1) was 4.7 times increased at this temperature range (550–600 °C) indicating the facilitated structural change from $\alpha\text{-MoO}_3$ or $\text{Mo}_2\text{O}_x\text{N}_{1-x}$ to Mo_2N . In addition, the induction period in the conversion of NH_3 was observed during the decomposition of NH_3 at all temperatures except 700 °C indicating that the transition of $\alpha\text{-MoO}_3$ or $\text{Mo}_2\text{O}_x\text{N}_{1-x}$ to Mo_2N still proceeds at the reaction condition.

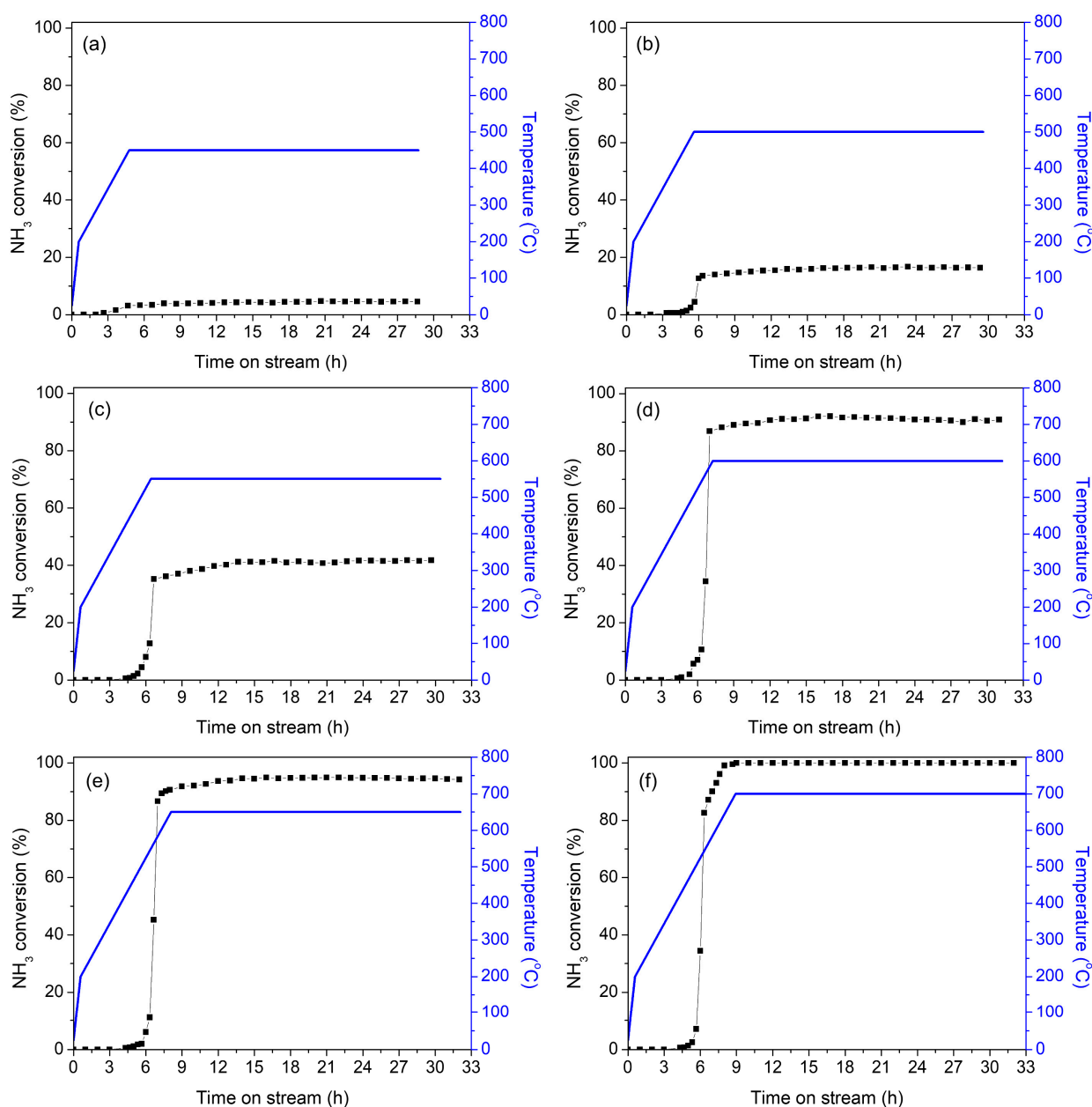


Figure 8. Evolution of NH_3 conversion during the temperature programmed nitridation of $\alpha\text{-MoO}_3$ at different temperatures in flowing pure ammonia, 3.4 L h^{-1} for 0.3 g of $\alpha\text{-MoO}_3$; (a) 450, (b) 500, (c) 550, (d) 600, (e) 650, and (f) 700 °C.

Figure 9a shows the XRD patterns of molybdenum nitride samples prepared at 650 °C for 7 and 24 h, respectively. It is obvious that the remaining portion of MoO₂ on the molybdenum nitride sample reduced at the prolonged reactions (nitridation and NH₃ decomposition). In addition, this further nitridation of sample during the reaction conditions results in the increase of both BET surface area and total pore volume (Figure 9b), which are favorable for the catalytic performance of molybdenum nitride (Figure 9c). The apparent activation energies (E_a) of ammonia decomposition between 400 and 525 °C over two molybdenum nitride samples prepared at 650 °C for nitridation times from 7 and 24 h were calculated using the following relationship: $-r_{\text{NH}_3} = k_0 \exp(E_a/RT)P_{\text{NH}_3}^\alpha$. Here, r_{NH_3} is the number of moles of NH₃ consumed per second per gram of base MoO₃. As shown in Figure 8a, the NH₃ conversion was higher over the sample prepared for a longer nitridation time, indicating that the nitridation period is another decisive parameter determining the catalytic activity of molybdenum nitrides. Figure 8b shows the Arrhenius plots for NH₃ consumption over the two molybdenum nitride catalysts. The apparent activation energies of ammonia decomposition were calculated to be 28.4 and 29.4 kcal/mol over the samples nitrided for 7 and 24 h, respectively. The activation energies of the molybdenum nitride catalysts were slightly higher than those of molybdenum carbide (21.3 kcal/mol) and supported Ru catalysts (17.9–20.3 kcal/mol) reported in the literature [47]. Overall, the results of this study reveal the potential of high surface area molybdenum nitrides as catalysts for H₂ production via ammonia decomposition.

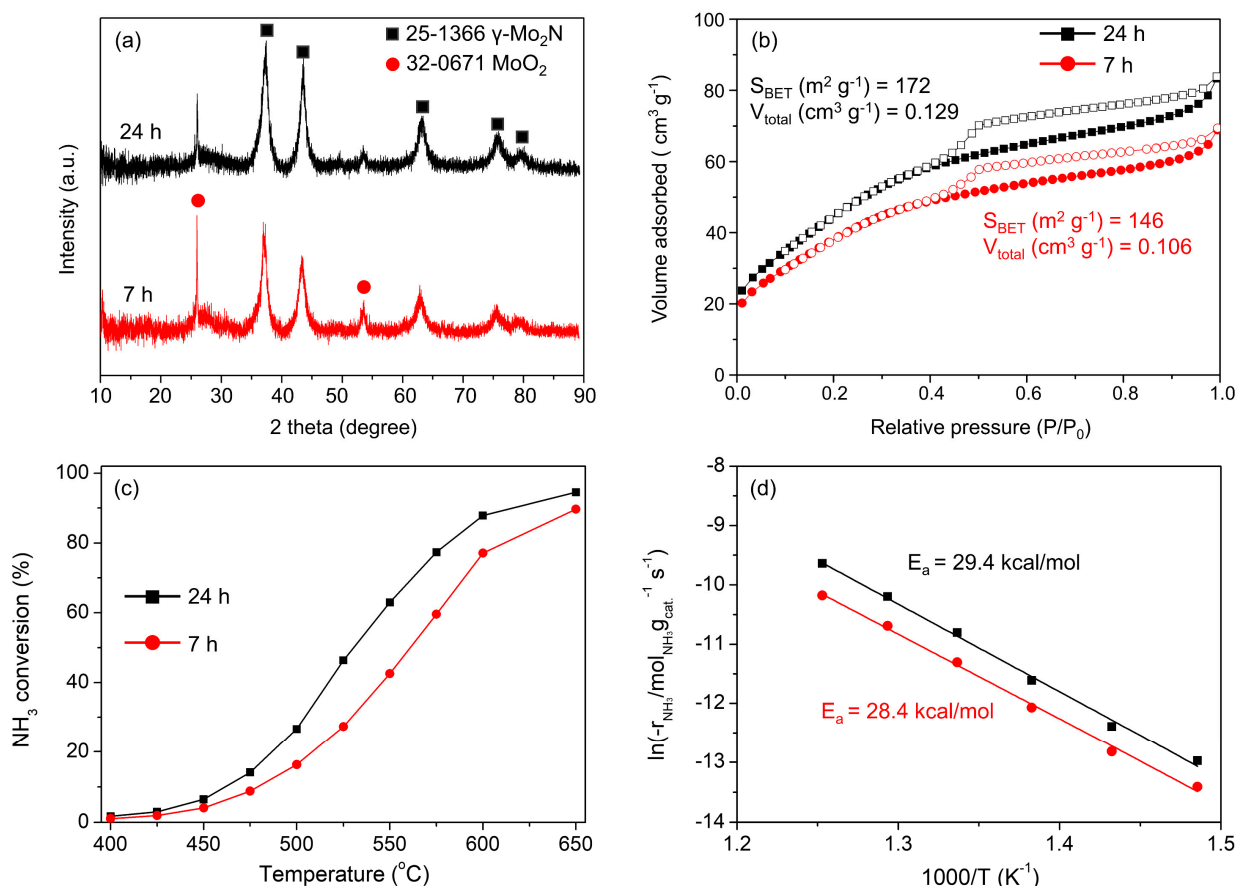


Figure 9. (a) XRD patterns, (b) N₂ adsorption-desorption isotherms, (c) catalytic activity of molybdenum nitride as a function of reaction temperature in the decomposition of ammonia, and (d) Arrhenius' plot of NH₃ consumption over molybdenum nitride catalysts from 400 to 525 °C. The molybdenum nitride samples were prepared in pure ammonia flow (3.4 L h⁻¹) using 0.3 g α -MoO₃ at heating rates of 5 °C min⁻¹ to 200 °C and 1 °C min⁻¹ to 650 °C followed by maintenance at that temperature for 7 or 24 h.

3. Experimental

3.1. Catalyst Preparation

Molybdenum nitride having a high specific surface area was synthesized by the temperature-programmed nitridation of α -MoO₃ (Sigma–Aldrich, St. Louis, MO, USA) in a flow of pure ammonia. The optimal synthetic parameters were investigated by changing the pure ammonia flow rate (2–11.5 L h^{−1}), heating rate (30–240 °C h^{−1}), and nitridation temperature (425–846 °C). The molar hourly space velocity (MHSV, h^{−1}) is defined as the molar flow rate of pure ammonia per mole of α -MoO₃ as the molybdenum nitride precursor. Typically, pure molybdenum nitride phase was obtained by the nitridation of α -MoO₃ at a reaction temperature of 700 °C for 7 h at a heating rate of 200 °C h^{−1} to 200 °C and 60 °C h^{−1} to 700 °C in flowing ammonia (10 L h^{−1} for 1 g of α -MoO₃, i.e., MHSV = 64.2 h^{−1}). After cooling, the samples to room temperature in flowing N₂ (100 cm³ g^{−1}), passivation was performed using 1% O₂/N₂ (100 cm³ min^{−1}) for a minimum of 1 h to avoid the rapid oxidation of the external nitride surface.

3.2. Catalyst Characterization

XRD analyses were performed to examine the crystal phases of the prepared catalysts using a D8 Discover with a GADDS detector (Bruker AXS, Billerica, MA, USA). The generator current and voltage were 30 mA and 50 kV, respectively, and Cu K_α X-rays (0.15418 nm) were used. The analyses were carried out between 2 θ values of 10° and 90° at a scanning rate of 0.4° min^{−1}. To measure the specific surface area, pore size distribution, and total pore volume of the catalyst used, nitrogen adsorption–desorption measurements were performed at liquid nitrogen temperature (−196 °C) using an ASAP 2020 (Micromeritics, Norcross, GA, USA). The specific surface area was measured in the relative pressure (P/P_0) range of 0.05–0.2 using the BET formula. The total pore volume was calculated from the amount of nitrogen adsorbed at $P/P_0 = 0.995$. The pore size distribution was calculated from the adsorption isotherm using the BJH equation. XPS measurements were performed on a PHI Quantera II analyzer (Al K_α = 1486.6 eV, Ulvac-PHI Inc., Chigasaki, Kanagawa, Japan), and the results were used to investigate the electronic states of the surface elements in the molybdenum nitride samples. The binding energy was corrected based on the C 1s peak at 284.6 eV. Changes in the morphology of the catalysts were observed through TEM, and elemental analyses of the catalyst were performed via EDS analysis. SAED measurements were performed to confirm the crystalline phases. An FEI/Talos F200X (Thermo Fisher Scientific, Waltham, MA, USA) was used for TEM measurements, and an Oxford X-Max⁵⁰ (Oxford Instruments, Abingdon-on-Thames, UK) was used for EDS analyses; Mn K_α radiation ($h\nu \leq 129$ eV) produced at an acceleration voltage of 200 kV was used. Samples used for TEM and EDS analyses were dispersed in toluene (>99.8%, SAMCHUN, Pyungtaek, Korea) for 5 min using a small fraction of the prepared catalyst. Temperature-programmed decomposition (TPD) experiments were performed to investigate the decomposition of molybdenum nitride in pure He, O₂, and 20% H₂/He at flow rates of 100 cm³ min^{−1}. The TPD experiments were carried out at room temperature to 700 °C at a heating rate of 10 °C min^{−1}, and the decomposed gases were analyzed by QMS 200 (Balzers, Nashua, NH, USA). Simultaneous TG-DTA (TA Instruments, New Castle, DE, USA) analyses of molybdenum nitride was performed in flowing helium, pure oxygen, and 20% H₂/He at flow rates of 50 cm³ min^{−1}.

3.3. Catalytic Activity Tests

The catalytic activity of molybdenum nitride prepared by the temperature-programmed nitridation of α -MoO₃ for ammonia decomposition was tested at atmospheric pressure. The conversion of ammonia is defined using Equation (1).

$$\text{Conversion of ammonia (\%)} = \frac{\frac{2}{3} F_{\text{H}_2} \text{ produced}}{F_{\text{NH}_3} \text{ fed}} \times 100 \quad (1)$$

Here, F_{H_2} and F_{NH_3} are the molar flow rates of produced hydrogen and reactant ammonia, respectively. The reactants and products (ammonia, hydrogen, and water) were analyzed using nitrogen as carrier gas and a gas chromatograph (Varian 450GC, Varian Inc., Palo Alto, CA, USA) equipped with a Carbosphere-packed column (1/8" × 1.8 m) and a thermal conductivity detector (TCD).

4. Conclusions

Temperature-programmed nitridation of α -MoO₃ was performed to prepare molybdenum nitride with a high surface area (>170 m² g⁻¹). MoO₂ was observed as the intermediate phase. A mixture of molybdenum metal and molybdenum nitride was observed by XRD analyses after the nitridation of α -MoO₃ at temperatures over 800 °C, and this phase transformation caused a rapid decrease in the specific surface area. When the prepared molybdenum nitride was exposed to air, the diffusion of oxygen into the bulk nitride resulted in a volume expansion, and a corresponding gradual reduction in the surface area and total pore volume arising from pore blocking was also observed. The easy diffusion of oxygen into the molybdenum nitride resulted in the formation of oxynitrides, but up to 90% of the initial specific surface area was recovered after H₂ treatment. The catalytic activity of molybdenum nitride for ammonia decomposition was dependent on the degree of nitridation, and, of the molybdenum nitride samples, that with the highest degree of nitridation showed the highest catalytic activity. The molybdenum nitride obtained by the nitridation at 650 °C for 24 h exhibits the conversion of ammonia higher than 94% at the same temperature without significant catalyst deactivation.

Supplementary Materials: The following are available online at <https://www.mdpi.com/2073-4344/11/2/192/s1>: Figure S1: XRD patterns of nitride samples obtained after nitridation of MoO₃ as a function of (a) reaction temperature and (b) MHSV (h⁻¹) at 650 °C. Standard nitridation conditions: pure ammonia flow rate of 3.36 L h⁻¹ for 0.3 g MoO₃ (MHSV = 72 h⁻¹) at heating rates of 200 °C h⁻¹ to 200 °C and 60 °C h⁻¹ to the final temperature, followed by maintenance at this temperature for 7 h. Figure S2: (a) XRD pattern of nitride sample and those after temperature-programmed decomposition of the nitride sample at (b) 700 °C at a heating rate of 10 °C min⁻¹ in flow of pure He (100 cm³ min⁻¹) and at (c) 700 °C at a heating rate of 10 °C min⁻¹ in flow of 5% O₂/He (100 cm³ min⁻¹). The nitride sample in (a) was obtained by the nitridation of MoO₃ under the following reaction conditions: reaction temperature of 700 °C for 7 h at a heating rate of 60 °C h⁻¹ in pure ammonia at a flow rate of 10 L h⁻¹ for 1 g of MoO₃ (MHSV = 64.2 h⁻¹). Figure S3: XRD patterns of molybdenum oxynitride samples exposed to air as a function of exposure time: (a) passivated samples after nitridation at 700 °C for (b) 3, (c) 5, and (d) 7 days; Figure S4: N₂ adsorption–desorption isotherms and pore size distribution of molybdenum nitride exposed to air for 60 days and (b) treated at 500 °C for 2 h in pure H₂ (30 cm³ min⁻¹); Table S1: Mass variation, chemical compositions, and XRD phases of nitride samples obtained after the nitridation of MoO₃ as a function of reaction temperature, heating rate, and MHSV. Nitridation was carried out at the final temperature for 7 h.

Author Contributions: Conceptualization: H.-K.M. and C.-H.S.; methodology: S.-H.B., K.Y., D.-C.K., H.-K.M., and C.-H.S.; investigation: S.-H.B., K.Y., D.-C.K., H.A., M.B.P., H.-K.M., and C.-H.S.; resources: S.-H.B., D.-C.K., and C.-H.S.; data curation: S.-H.B., K.Y., and D.-C.K.; writing—original draft preparation: S.-H.B., K.Y., and D.-C.K.; writing—review and editing: S.-H.B., K.Y., and D.-C.K.; supervision: H.-K.M. and C.-H.S.; project administration: H.-K.M. and C.-H.S.; funding acquisition: C.-H.S. All authors have read and agreed to the published version of the manuscript.

Funding: This research was funded by the Research Year of Chungbuk National University in 2020 and the C1 Gas Refinery Program through the National Research Foundation of Korea (NRF) funded by the Ministry of Science, ICT and Future Planning (2015M3D3A1A01064899).

Institutional Review Board Statement: Not applicable.

Informed Consent Statement: Not applicable.

Data Availability Statement: Not applicable.

Conflicts of Interest: The authors declare no conflict of interest.

References

1. Alexander, A.-M.; Hargreaves, J.S.J. Alternative catalytic materials: Carbides, nitrides, phosphides and amorphous boron alloys. *Chem. Soc. Rev.* **2010**, *39*, 4388–4401. [[CrossRef](#)] [[PubMed](#)]
2. Kung, H.H. *Transition Metal Oxides: Surface Chemistry and Catalysis*; Elsevier: Burlington, MA, USA, 1989; Volume 45.
3. Kral, C.; Lengauer, W.; Rafaja, D.; Ettmayer, P. Critical review on the elastic properties of transition metal carbides, nitrides and carbonitrides. *J. Alloys Compd.* **1998**, *265*, 215–233. [[CrossRef](#)]
4. Oyama, S.T. Transition Metal Carbides, Nitrides, and Phosphides. In *Handbook of Heterogeneous Catalysis*, 2nd ed.; Ertl, G., Knözinger, H., Weitkamp, J., Eds.; Wiley-VCH, Cop.: Weinheim, Allemagne, 2008; Volume 8, pp. 342–355.
5. Jagers, C.H.; Michaels, J.N.; Stacy, A.M. Preparation of high-surface-area transition-metal nitrides: Molybdenum nitrides, Mo₂N and MoN. *Chem. Mater.* **1990**, *2*, 150–157. [[CrossRef](#)]
6. Volpe, L.; Boudart, M. Compounds of molybdenum and tungsten with high specific surface area: I. Nitrides. *J. Solid State Chem.* **1985**, *59*, 332–337. [[CrossRef](#)]
7. Volpe, L.; Boudart, M. Compounds of molybdenum and tungsten with high specific surface area: II. Carbides. *J. Solid State Chem.* **1985**, *59*, 338–356. [[CrossRef](#)]
8. Shin, C.-H.; Bugli, G.; Djéga-Mariadassou, G. Preparation and characterization of titanium oxynitrides with high specific surface areas. *J. Solid State Chem.* **1991**, *95*, 145–155. [[CrossRef](#)]
9. Tomas-Garcia, A.L.; Li, Q.; Jensen, J.O.; Bjerrum, N.J. High surface area tungsten carbides: Synthesis, characterization and catalytic activity towards the hydrogen evolution reaction in phosphoric acid at elevated temperatures. *Int. J. Electrochem. Sci.* **2014**, *9*, 1016–1032.
10. Iglesia, E.; Ribeiro, F.H.; Boudart, M.; Baumgartner, J.E. Synthesis, characterization, and catalytic properties of clean and oxygen-modified tungsten carbides. *Catal. Today* **1992**, *15*, 307–337. [[CrossRef](#)]
11. Podila, S.; Zaman, S.F.; Driss, H.; Alhamed, Y.A.; Al-Zahrani, A.A.; Petrov, L.A. Hydrogen production by ammonia decomposition using high surface area Mo₂N and Co₃Mo₃N catalysts. *Catal. Sci. Technol.* **2016**, *6*, 1496–1506. [[CrossRef](#)]
12. Podila, S.; Zaman, S.F.; Driss, H.; Al-Zahrani, A.A.; Daous, M.A.; Petrov, L.A. High performance of bulk Mo₂N and Co₃Mo₃N catalysts for hydrogen production from ammonia: Role of citric acid to Mo molar ratio in preparation of high surface area nitride catalysts. *Int. J. Hydrogen Energy* **2017**, *42*, 8006–8020. [[CrossRef](#)]
13. Li, Y.; Zhang, Y.; Raval, R.; Li, C.; Zhai, R.; Xin, Q. The modification of molybdenum nitrides: The effect of the second metal component. *Catal. Lett.* **1997**, *48*, 239–245. [[CrossRef](#)]
14. Srifa, A.; Okura, K.; Okanishi, T.; Muroyama, H.; Matsui, T.; Eguchi, K. CO_x-free hydrogen production via ammonia decomposition over molybdenum nitride-based catalysts. *Catal. Sci. Technol.* **2016**, *6*, 7495–7504. [[CrossRef](#)]
15. Klerke, A.; Christensen, C.H.; Norskov, J.K.; Vegge, T. Ammonia for hydrogen storage: Challenges and opportunities. *J. Mat. Chem.* **2008**, *18*, 2304–2310. [[CrossRef](#)]
16. Zamfirescu, C.; Dincer, I. Using ammonia as a sustainable fuel. *J. Power Sources* **2008**, *185*, 459–465. [[CrossRef](#)]
17. Mukherjee, S.; Devaguptapu, S.V.; Sviripa, A.; Lund, C.R.F.; Wu, G. Low-temperature ammonia decomposition catalysts for hydrogen generation. *Appl. Catal. B Environ.* **2018**, *226*, 162–181. [[CrossRef](#)]
18. Hill, A.K.; Torrente-Murciano, L. Low temperature H₂ production from ammonia using ruthenium-based catalysts: Synergetic effect of promoter and support. *Appl. Catal. B Environ.* **2015**, *172–173*, 129–135. [[CrossRef](#)]
19. Yin, S.-F.; Zhang, Q.-H.; Xu, B.-Q.; Zhu, W.-X.; Ng, C.-F.; Au, C.-T. Investigation on the catalysis of CO_x-free hydrogen generation from ammonia. *J. Catal.* **2004**, *224*, 384–396. [[CrossRef](#)]
20. Duan, X.; Qian, G.; Zhou, X.; Sui, Z.; Chen, D.; Yuan, W. Tuning the size and shape of Fe nanoparticles on carbon nanofibers for catalytic ammonia decomposition. *Appl. Catal. B Environ.* **2011**, *101*, 189–196. [[CrossRef](#)]
21. Bell, T.E.; Torrente-Murciano, L. H₂ production via ammonia decomposition using non-noble metal catalysts: A review. *Top. Catal.* **2016**, *59*, 1438–1457. [[CrossRef](#)]
22. Gurram, V.R.B.; Enumula, S.S.; Chada, R.R.; Koppadi, K.S.; Burri, D.R.; Kamaraju, S.R.R. Synthesis and industrial catalytic applications of binary and ternary molybdenum nitrides: A review. *Catal. Surv. Asia* **2018**, *22*, 166–180. [[CrossRef](#)]
23. Lendzion-Bielun, Z.; Narkiewicz, U.; Arabczyk, W. Cobalt-based catalysts for ammonia decomposition. *Materials* **2013**, *6*, 2400–2409. [[CrossRef](#)] [[PubMed](#)]
24. Zeinalipour-Yazdi, C.D.; Hargreaves, J.S.J.; Catlow, C.R.A. Low-T Mechanisms of ammonia synthesis on Co₃Mo₃N. *J. Phys. Chem. C* **2018**, *122*, 6078–6082. [[CrossRef](#)]
25. McKay, D.; Hargreaves, J.S.J.; Rico, J.L.; Rivera, J.L.; Sun, X.-L. The influence of phase and morphology of molybdenum nitrides on ammonia synthesis activity and reduction characteristics. *J. Solid State Chem.* **2008**, *181*, 325–333. [[CrossRef](#)]
26. Nishiyashi, Y. Molybdenum-catalyzed reduction of molecular dinitrogen into ammonia under ambient reaction conditions. *C.R. Chimie* **2015**, *18*, 776–784. [[CrossRef](#)]
27. Nagai, M.; Goto, Y.; Miyata, A.; Kiyoshi, M.; Hada, K.; Oshikawa, K.; Omi, S. Temperature-programmed reduction and XRD studies of ammonia-treated molybdenum oxide and its activity for carbazole hydrodenitrogenation. *J. Catal.* **1992**, *182*, 292–301. [[CrossRef](#)]
28. Li, S.; Lee, J.S. Molybdenum nitride and carbide prepared from heteropolyacid. II. Hydrodenitrogenation of indole. *J. Catal.* **1998**, *173*, 134–144.

29. Chen, X.; Zhang, T.; Zheng, M.; Wu, Z.; Wu, W.; Li, C. The reaction route and active site of catalytic decomposition of hydrazine over molybdenum nitride catalyst. *J. Catal.* **2004**, *224*, 473–478. [[CrossRef](#)]
30. He, H.; Dai, H.X.; Ngan, K.Y.; Au, C.T. Molybdenum nitride for the direct decomposition of NO. *Catal. Lett.* **2001**, *71*, 147–153. [[CrossRef](#)]
31. Inumaru, K.; Baba, K.; Yamanaka, S. Synthesis and characterization of superconducting β -Mo₂N crystalline phase on a Si substrate: An application of pulsed laser deposition to nitride chemistry. *Chem. Mater.* **2005**, *17*, 5935–5940. [[CrossRef](#)]
32. Dewangan, K.; Patil, S.S.; Joag, D.S.; More, M.A.; Gajbhiye, N.S. Topotactical nitridation of α -MoO₃ fibers to γ -Mo₂N fibers and its field emission properties. *J. Phys. Chem. C* **2010**, *114*, 14710–14715. [[CrossRef](#)]
33. Wei, Z.B.; Xin, Q.; Grange, P.; Delmon, B. Surface species and the stability of γ -Mo₂N. *Solid State Ion.* **1997**, *101–103*, 761–767. [[CrossRef](#)]
34. Cárdenas-Lizana, F.; Gómez-Quero, S.; Perret, N.; Kiwi-Minsker, L.; Keane, M.A. β -Molybdenum nitride: Synthesis mechanism and catalytic response in the gas phase hydrogenation of p-chloronitrobenzene. *Catal. Sci. Technol.* **2011**, *1*, 794–801.
35. Cárdenas-Lizana, F.; Lamey, D.; Kiwi-Minsker, L.; Keane, M.A. Molybdenum nitrides: A study of synthesis variables and catalytic performance in acetylene hydrogenation. *J. Mater. Sci.* **2018**, *53*, 6707–6718. [[CrossRef](#)]
36. Gong, S.; Chen, H.; Li, W.; Li, B. Synthesis of β -Mo₂N_{0.78} hydrodesulfurization catalyst in mixtures of nitrogen and hydrogen. *Appl. Catal. A Gen.* **2005**, *279*, 257–261. [[CrossRef](#)]
37. Choi, J.-G.; Brenner, J.R.; Colling, C.W.; Demczyk, B.G.; Dunning, J.L.; Thompson, L.T. Synthesis and characterization of molybdenum nitride hydrodenitrogenation catalysts. *Catal. Today* **1992**, *15*, 201–222. [[CrossRef](#)]
38. Spevack, P.A.; McIntyre, N.S. Thermal reduction of molybdenum trioxide. *J. Phys. Chem.* **1992**, *96*, 9029–9035. [[CrossRef](#)]
39. Gregg, S.J.; Sing, K.S.W. *Adsorption, Surface Area and Porosity*; Academic Press: London, UK, 1982; ISBN 9780123009500.
40. Chen, J.; Wei, Q. Phase transformation of molybdenum trioxide to molybdenum dioxide: An in-situ transmission electron microscopy investigation. *Int. J. Appl. Ceram. Technol.* **2017**, *14*, 1020–1025. [[CrossRef](#)]
41. Choi, J.-G.; Curl, R.L.; Thompson, L.T. Molybdenum nitride catalysts I. Influence of the synthesis factors on structural properties. *J. Catal.* **1994**, *146*, 218–227. [[CrossRef](#)]
42. Lee, K.-H.; Lee, Y.-W.; Kwak, D.-H.; Moon, J.-S.; Park, A.-R.; Hwang, E.-T.; Park, K.-W. Single-crystalline mesoporous Mo₂N nanobelts with an enhanced electrocatalytic activity for oxygen reduction reaction. *Mater. Lett.* **2014**, *124*, 231–234.
43. Clayton, C.R. *Passivity Mechanisms in Stainless Steels: Mo-N Synergism*; State University of New York at Stony Brook, Department of Materials Science and Engineering, Stony Brook: New York, NY, USA, 1986.
44. Yuan, Y.; Zhang, B.; Sun, J.; Jonnard, P.; Le Guen, K.; Tu, Y.; Yan, C.; Lan, R. Structure and optical properties of CrOxNy films with composition modulation. *Surf. Eng.* **2019**, *36*, 411–417. [[CrossRef](#)]
45. Su, D.; Zhang, X.; Wu, A. CoO-Mo₂N hollow heterostructure for high-efficiency electrocatalytic hydrogen evolution reaction. *NPG Asia Mater.* **2019**, *11*, 78. [[CrossRef](#)]
46. Wei, Z.B.Z.; Grange, P.; Delmon, B. XPS and XRD studies of fresh and sulfided Mo₂N. *Appl. Surf. Sci.* **1998**, *135*, 107–114. [[CrossRef](#)]
47. Zheng, W.; Cotter, T.P.; Kaghazchi, P.; Jacob, T.; Frank, B.; Schlichte, K.; Zhang, W.; Su, D.S.; Schüth, F.; Schlögl, R. Experimental and theoretical investigation of molybdenum carbide and nitride as catalysts for ammonia decomposition. *J. Am. Chem. Soc.* **2013**, *135*, 3458–3464. [[CrossRef](#)] [[PubMed](#)]